Chapter 2—Description of Cavity Ringdown Spectrometer

Experimental apparatus section: Reproduced in part with permission from Sprague et al.,[31] Copyright 2012 American Chemical Society.

Abstract

Cavity ringdown spectroscopy (CRDS) is a sensitive technique that makes use of an optical cavity to measure absorptions on the order of parts per million. By choosing appropriate tunable light sources, we can measure the spectroscopy and kinetics of the chemical systems described in Chapter 1. This chapter summarizes the operating principles and specifications of our cavity ringdown spectrometer. Tunable infrared light is generated by sending the output of a Nd:YAG pumped dye laser into either an optical parametric amplifier or a hydrogen-filled Raman shifter. The infrared light is sent into the gas kinetics and ringdown cell. Radical chemistry is initiated by pulsed laser photolysis of precursor chemicals using an excimer laser. To assess the performance of the spectrometer, laser power, pulse energy fluctuations, timing jitter, mirror reflectivity, and minimum detectable absorbance were all measured. The spectrometer was calibrated using known spectroscopic lines and a readout on the dye laser indicating its position.

Introduction

Cavity Ringdown Spectroscopy

Absorption spectroscopy is governed by the Beer-Lambert Law:

$$A = \ln\left(\frac{I_0}{I}\right) = \sigma L_{abs} N \,, \tag{2.1}$$

where A is the absorbance, I_0 is the initial light intensity, I is the transmitted light intensity, σ is the absorption cross section, L_{abs} is the path length of light through the absorber, and N is the number density of absorber molecules (per unit volume). For molecules with small cross sections, a detectable absorbance can be attained by two methods: increasing the concentration of absorber molecules, or by increasing the physical absorption path length using long pass absorption spectroscopy.

In many cases, neither of these options is viable. Increasing the concentration of chemical absorbers in radical chemistry studies can lead to unwanted secondary chemistry effects. For example, consider a kinetics experiment on the reaction of the hydroperoxy radical (HO_2) with an excess amount of formaldehyde (HCHO), the chemical system described in Part 2 of this thesis. The goal of the study is to determine the rate constant of the reaction between HO_2 and HCHO. If these two chemicals are the only reactive species present, then two possible reactions can occur:

$$HO_2\bullet + HCHO \rightarrow HOCH_2OO\bullet, \tag{2.2}$$

$$HO_2\bullet + HO_2\bullet \xrightarrow{(+M)} H_2O_2 + O_2. \tag{2.3}$$

Since HO_2 is consumed in both reactions, and HCHO is in excess, we must measure the formation of $HOCH_2OO\bullet$ in order to determine the rate constant for Reaction 2.2. One way to do this is to measure the OH stretch spectrum of $HOCH_2OO\bullet$. In order to obtain a detectable concentration of $HOCH_2OO\bullet$, we could increase $[HO_2]$. This will, however, also increase the rate of Reaction 2.3, producing H_2O_2, a chemical that will interfere with the spectroscopic detection of $HOCH_2OO\bullet$. A doubling of $[HO_2]$ will double the rate of Reaction 2.2, but quadruple the rate of Reaction 2.3. At high concentrations, the only product that will be detected is H_2O_2, making the kinetics experiment impossible.

Additionally, increasing the physical sample path length is often cumbersome or impossible. For the chemical systems studied in our laboratory, photolysis of precursor chemicals is necessary to generate the reactants necessary to initiate chemistry. Using a long pass cell would prove unwieldy, as the photolysis beam would need a very large flux in order to photolyze precursors in the entire cell. For example, consider a 10 m long White cell with a minimum detectable absorbance of 10^{-5} used for detecting the OH stretch of the δ-HOC_4H_8• radical (σ_{peak} = 7.5 × 10^{-20} cm^2), one of the alkoxy isomerization products discussed in Part 4 of this thesis. The minimum concentration of reactant radicals necessary for detection is 1.3 × 10^{11} molecules cm^{-3}, which is low enough to prevent secondary chemistry effects. However, these reactant radicals are generated from photolysis of precursor alkyl nitrites, with a UV cross section of 8 × 10^{-20} cm^2 at 351 nm.[32] In order to prevent secondary chemistry due to the presence of excess alkyl nitrites, a typical experiment aims for 1% photolysis. This requires a photon flux of 1.0 × 10^{17} cm^{-2}. For a 10 m long cell and a 0.5 cm high photolysis beam, a laser with an energy output of 32 J/pulse is required. Even if such a high powered laser was commercially available, it would be dangerous to operate and uneconomical to purchase.

Since neither long-pass absorption spectroscopy nor increasing the radical concentrations are acceptable ways to improve sensitivity, we must take a different approach. One way to do this is by increasing the effective path length via an optical cavity. Cavity ringdown spectroscopy (CRDS)[6-11, 33] is a suitable experimental technique for detection of small absorbances. The technique requires two highly reflective mirrors (R > 99.9%) to create an optical cavity. Laser light is injected into the cavity, and the small amount of light that is transmitted through the mirrors is detected. The intensity of

the transmitted light is proportional to the intensity of light in the cavity. Over time, the amount of light reaching the detector decays exponentially. This decay is called "ringdown," named such because of the similarity to the sound decay of a ringing bell.

If the only loss process for light is leakage through the mirrors, the ringdown is characterized by

$$I = I_0 \exp\left(\frac{-t}{\tau_0}\right), \text{ with } \tau_0 = \frac{t_r}{2(1-R)} = \frac{L_{opt}}{c(1-R)}, \tag{2.4}$$

where t_r is the roundtrip time for light in the cavity, R is the mirror reflectivity, L_{opt} is the distance between the two mirrors, c is the speed of light, and τ_0 is the 1/e decay time of the light (called the ringdown lifetime).

When an absorber is present in the cavity, Equation 2.4 must be modified to

$$I = I_0 \exp\left(-\frac{t}{\tau}\right), \text{ with } \frac{1}{\tau} = \frac{1}{\tau_0} + \left(\sigma L_{abs} N\right)\left(\frac{c}{L_{opt}}\right), \tag{2.5}$$

where L_{abs} is the path length of the absorber and τ is the 1/e decay time for light in the presence of the absorber. The absorbance can be calculated from equations 2.4 and 2.5:

$$A = \frac{L_{opt}}{c}\left(\frac{1}{\tau} - \frac{1}{\tau_0}\right). \tag{2.6}$$

Equation 2.6 is valid for comparison of a cavity in the presence of chemical absorbers (with ringdown time τ) to a cavity in a reference state without the chemical absorbers (with ringdown time τ_0). The reference state does not necessarily have to be an empty cavity. For an experiment in which photolysis initiates chemistry, the reference state is chosen to be the cavity filled with reactant gases, prior to photolysis. By choosing this reference state, we effectively subtract out any background absorption from the

precursor chemicals. Ringdown decays are measured before and after photolysis. These decays are fit to a single exponential to calculate the characteristic lifetimes τ_0 and τ. By carefully controlling the time between photolysis and measuring the ringdowns, formation of photolysis products can be monitored.

To illustrate a typical ringdown measurement, we can examine the R(3) line of the ν_1 absorption of HO_2.[34-36] Figure 2.1 shows two ringdown traces obtained at 3525.2 cm^{-1}, in the absence (blue curve) and presence (pink curve) of HO_2. The traces have been normalized to the same peak voltage. Note that when HO_2 is present, the intensity of light reaching the detector decays faster, indicating absorption. The ringdown lifetimes are τ_0 = 3.95 μs (without HO_2), and τ = 3.75 μs with HO_2. Using Equation 2.6 (L_{opt} = 55 cm), we obtain an absorbance of 25 ppm for this HO_2 line. This is a relatively large absorption to measure with CRDS. For very large absorptions ($A > 0.1\times(1-R)$) and very sharp spectral peaks (less than 1/400 of the light's linewidth), equations 4–6 are not quantitatively correct. To obtain accurate absorbances, correction factors must be applied to the CRDS data.[11, 30]

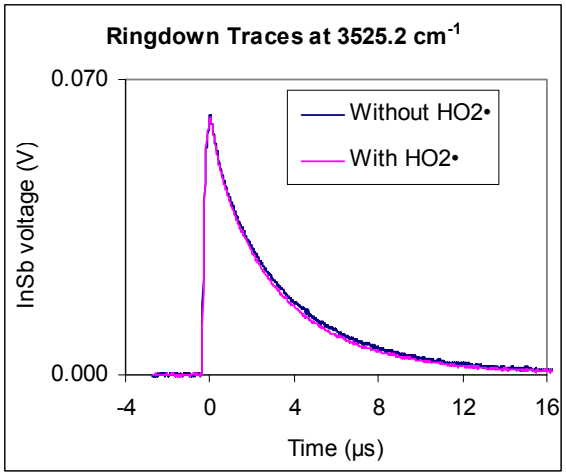

Figure 2.1. Sample ringdown traces at 3525.2 cm^{-1} in the absence of HO_2 (blue line, top) and in the presence of HO_2 (pink line, bottom). This frequency corresponds to the R(3) line of the ν_1 absorption of HO_2.[34-36] The two traces have been normalized to the same peak voltage. The ringdown lifetimes are τ_0 = 3.95 μs (without HO_2) and τ = 3.75 μs, giving an absorbance by HO_2 of 25 ppm (L_{opt} = 55 cm).

Pulsed ringdown systems (such as the one used for the work in this thesis) typically can obtain sensitivities of 0.1–1 ppm $Hz^{-½}$, depending on mirror reflectivity, optical cavity length, and absorption by background gases.[37] This is approximately three orders of magnitude more sensitive than a single-pass direct absorption method. It is possible for multipass absorption methods such as cavity enhanced absorption spectroscopy (CEAS) to approach the sensitivity of pulsed ringdown.[38] However, CRDS has a distinct advantage over CEAS and traditional absorption techniques. CRDS measurements are insensitive to laser power fluctuations because only the rate of signal decay is the quantity of interest. In contrast, CEAS and traditional absorption methods rely on the absolute signal intensity, making these methods susceptible to laser power fluctuations.

It is possible to obtain greater sensitivity using continuous wave light sources (cw-CRDS, sensitivity 1 ppb), or by combining an optical cavity with frequency

modulation detection (NICE-OHMS, sensitivity 1 ppt).[39] However, these methods come with their own drawbacks. Both methods require a continuous wave light source, such as a diode laser. Diode lasers generally have a smaller range of tunability than can be achieved in a pulsed light source system, making diode lasers inappropriate for use in preliminary spectroscopic studies. Additionally, NICE-OHMS is only an appropriate technique for very weak absorptions. If an absorption line is too strong, too much power will build up in the cavity, causing the detector signal to saturate.

Considerations of Tunable Light Ranges

The ranges of tunable light required for our experiments are determined by the properties of the atmospheric species being studied. Two functional groups are prevalent in the chemical systems described in Chapter 1: hydroxy groups (-OH) and peroxy groups (-OO•). Hydroxy groups are formed through reaction of organic species with HO_x. Peroxy groups are present in the atmosphere due to association reactions of oxygen with radical species.[1-3] A spectrometer with the ability to detect molecules containing these two functional groups can be used to study a wide variety of atmospherically relevant reactions.

Molecules with either of these two functional groups have distinct features in their spectra. Species containing a hydroxy group will have spectra with a broad, generally structureless peak around 2.7 μm (3680 cm^{-1}), resulting from the molecule's OH stretch normal mode. The position of this peak is sensitive to hydrogen bonding. A free OH group (i.e., not hydrogen bound) will have an OH stretch frequency near 3680 cm^{-1}, as observed in gas phase methanol.[40] However, a hydrogen bound OH group will have a

red-shifted OH stretch frequency, by as much as 400 cm^{-1}. This effect is most pronounced in condensed phase spectra; for example, liquid phase methanol has an OH stretch frequency of 3328 cm^{-1}.[41] However, the effect is also important in gas phase molecules with internal hydrogen bonding, such as peroxynitrous acid (HOONO). The magnitude of these frequency shifts can be highly dependent on molecular geometry and the excitation of other modes, possibly leading to sequence band formation over a range of hundreds of wavenumbers.[42, 43] Measurement of OH stretch groups therefore requires a large range of light tunability.

Species containing a peroxy group will have spectra with a weak, highly structured peak around 1.3 μm (7400 cm^{-1}). This peak arises from the first electronic ($\tilde{A}-\tilde{X}$) transition. The position of this peak is sensitive to the local chemical environment of the peroxy group. Alkane chain length and proximity to different functional groups can change the electronic transition frequency by ± 500 cm^{-1}.[44, 45] Furthermore, different conformers of the same molecule can have vastly different transition frequencies, by as much as 1000 cm^{-1}, as observed in the hydroxymethylperoxy radical (Part 3 of this thesis). The large shifts in $\tilde{A}-\tilde{X}$ transition frequency also highlight the need for a wide range of tunability.

Taking the above factors into account, we choose two techniques to generate light in two frequency ranges. To measure OH stretch spectra, we use optical parametric amplification to obtain tunable light over the range 2.7–3.7 μm. To measure the peroxy $\tilde{A}-\tilde{X}$ spectra, we use a hydrogen gas Raman shifter to obtain tunable light over the range 1.2–1.4 μm.

Optical Parametric Amplification: Mid-IR light (2.7-3.7 μm)

An optical parametric amplifier (OPA) system is used to obtain 2.7-3.7 μm light.[46, 47] A basic schematic of an OPA system is shown in Figure 2.2.

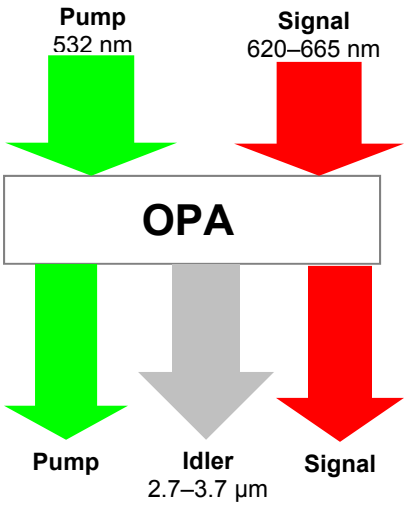

Figure 2.2. Schematic of an optical parametric amplifier (OPA). The wavelengths listed for the pump, signal, and idler beams are the wavelengths used in our apparatus. Note that in actual operation, the pump and signal beams are spatially and temporally matched.

A signal beam and a pump beam (of shorter wavelength than the signal beam) are sent through a nonlinear medium. Both beams must be matched spatially and temporally. Inside of the nonlinear medium, some of the pump beam photons are converted into two photons: one photon of the signal beam wavelength, and a second photon (idler) with a wavelength corresponding to the difference in pump and signal photon energies. In our setup, the pump photons are a fixed wavelength (532 nm), and the signal photons have a tunable wavelength (620-665 nm). Because the signal photons are tunable, the resulting idler photons are also tunable (2.7–3.7 μm). Our OPA typically produces 1 mJ of idler light, for 160 mJ of pump energy and 9 mJ of signal energy. The idler linewidth is 1 cm^{-1},

limited by the linewidth of the pump (1 cm^{-1}). Further details about the OPA system can be found in the *Experimental Details* section.

Hydrogen Gas Raman Shifter: Near-IR light (1.2–1.4 μm)

Our second method for generating tunable infrared light is to use a hydrogen gas Raman shifter. This setup gives us tunable light in the range 1.2–1.4 μm. A Raman shifter converts light from one wavelength to another by making use of the Raman effect. Figure 2.3 contains an energy diagram illustrating the Raman effect.

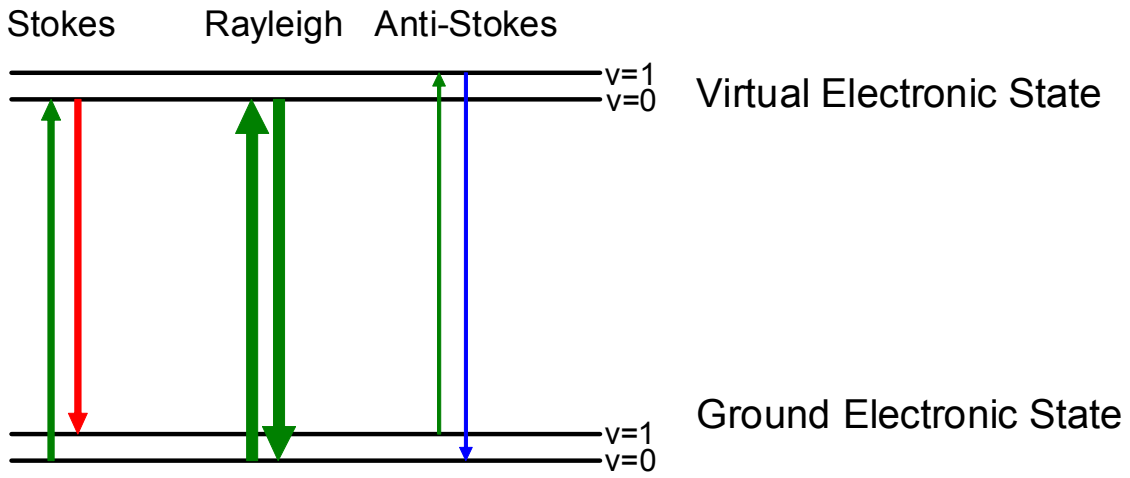

Figure 2.3. Energy diagram illustrating the Raman effect. Light of a given frequency excites polarizable molecules to a virtual state. The light produced when the molecule relaxes back to the ground state can be of lower frequency than the input (Stokes shifted), the same frequency as the input (Rayleigh scattered), or of higher frequency than the input (anti-Stokes shifted). The figure shows first Stokes and first anti-Stokes shifts. In our apparatus, we make use of the second Stokes shift in hydrogen gas (total shift 8310.4 cm^{-1}) to convert 620–665 nm light into 1.2–1.4 μm light.

When light enters a medium comprised of polarizable molecules, the molecules can be excited to virtual states. When the excited molecules relax back to their ground state, they can emit light of higher frequency (anti-Stokes shifted light), the same frequency (Rayleigh scattering), or lower frequency (Stokes shifted light). The frequency

shift between the incident and shifted photons is dependent on the medium used. We utilize hydrogen gas, which has a frequency shift is 4155.2 cm^{-1}. In our setup, the incident light is tunable over the range 620-665 nm. The second Stokes shifted light (total shift of 8310.4 cm^{-1}) gives us photons in the range 1.2-1.4 μm. The total energy of the Raman shifted light varies exponentially with the path length through the Raman shifter and incident power,[48] thus making multipass Raman shifter cells desirable. Additionally, focusing the beam within the Raman cell will also increase the energy of Raman shifted light. Our Raman shifter typically produces 90 μJ of infrared light for 30 mJ of incident red light. The linewidth of the Raman shifted light is 0.1 cm^{-1}, the same as the incident light. Further details of our Raman apparatus can be found in the *Experimental Details* section.

Experimental Details

Pulsed Laser Photolysis-Cavity Ringdown Spectroscopy (PLP-CRDS) Apparatus

The PLP-CRDS apparatus that was used in this thesis is the end result of 15 years of construction and repairs. Todd Fuelberth[49] and Eva Garland[29] constructed the optical parametric amplifier system currently in use. Andrew Mollner[30] installed the current excimer laser and gas flow system. My work has focused on laser installations and repair (see Part 5 of this thesis), replacement of the vacuum pump, and installation of the Raman shifter.

Figures 2.4 and 2.5 contain diagrams of the optical cavity and the two gas kinetics cells used. Figures 2.6 and 2.7 contain diagrams of the laser system. A full discussion of each component of the spectrometer can be found below; however, a brief overview is

warranted to orient the reader to each part of the spectrometer. The gas kinetics cells were constructed of stainless steel or quartz, with flat quartz windows to allow for the photolysis of chemicals within the cell. The cell was coupled to an optical cavity via mirror mounts. Light for the spectrometer was generated from Nd:YAG and dye lasers. To generate mid-infrared light, the Nd:YAG and dye laser outputs were mixed within an optical parametric amplifier. To generate near-infrared light, the dye laser output was sent through a hydrogen gas Raman shifter. An excimer laser was used to photolyze the chemicals within the kinetics cell. Digital delay generators controlled the timing between the excimer and Nd:YAG pulses. Ringdown data were collected using a photodiode connected to a PC oscilloscope.

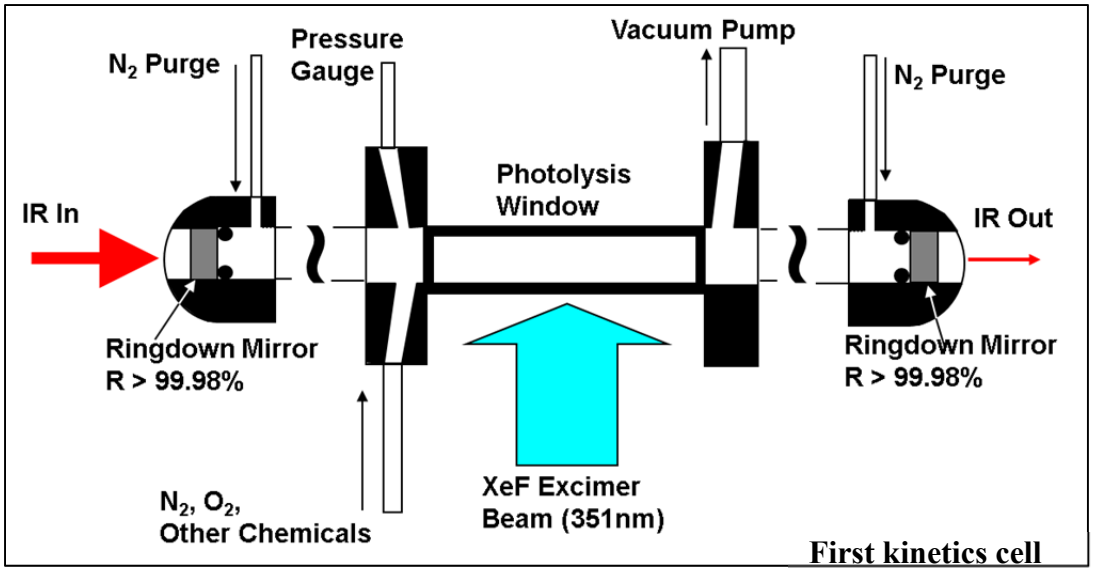

Figure 2.4. Diagram of the first kinetics cell (room temperature only).

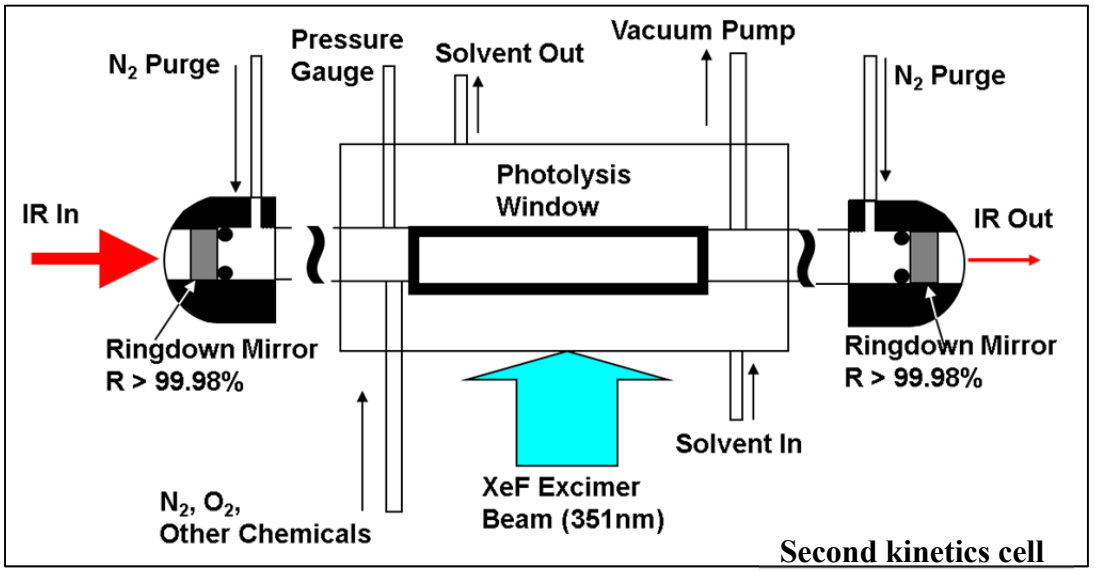

Figure 2.5. Diagram of the second kinetics cell (capable of temperature control).

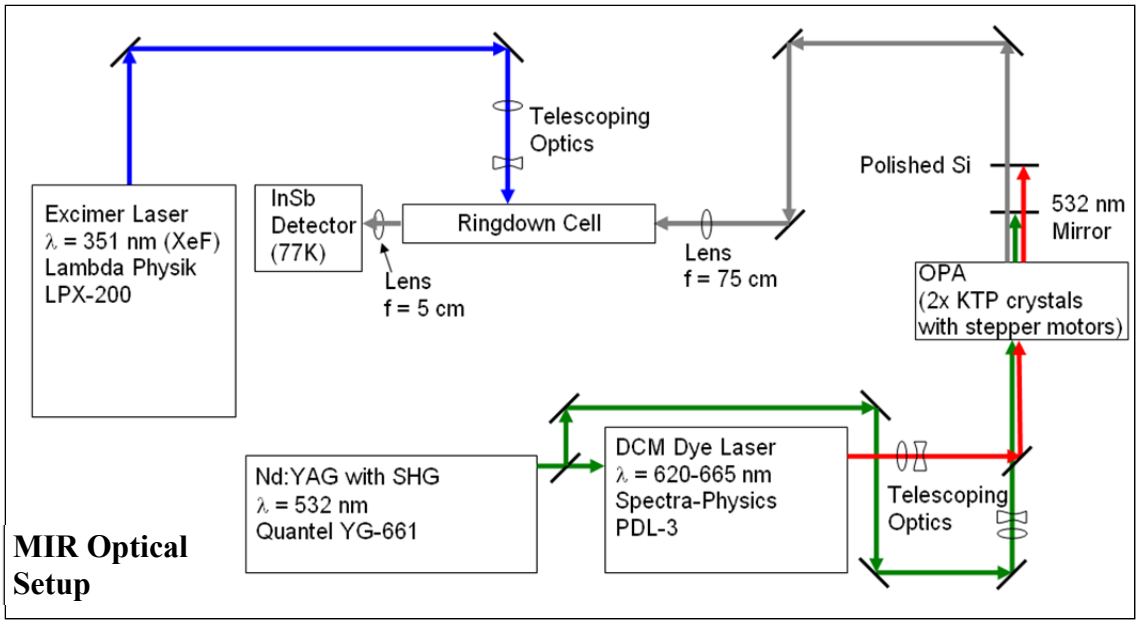

Figure 2.6. Optical setup for mid-infrared light (2.7–3.7 μm, using the OPA).

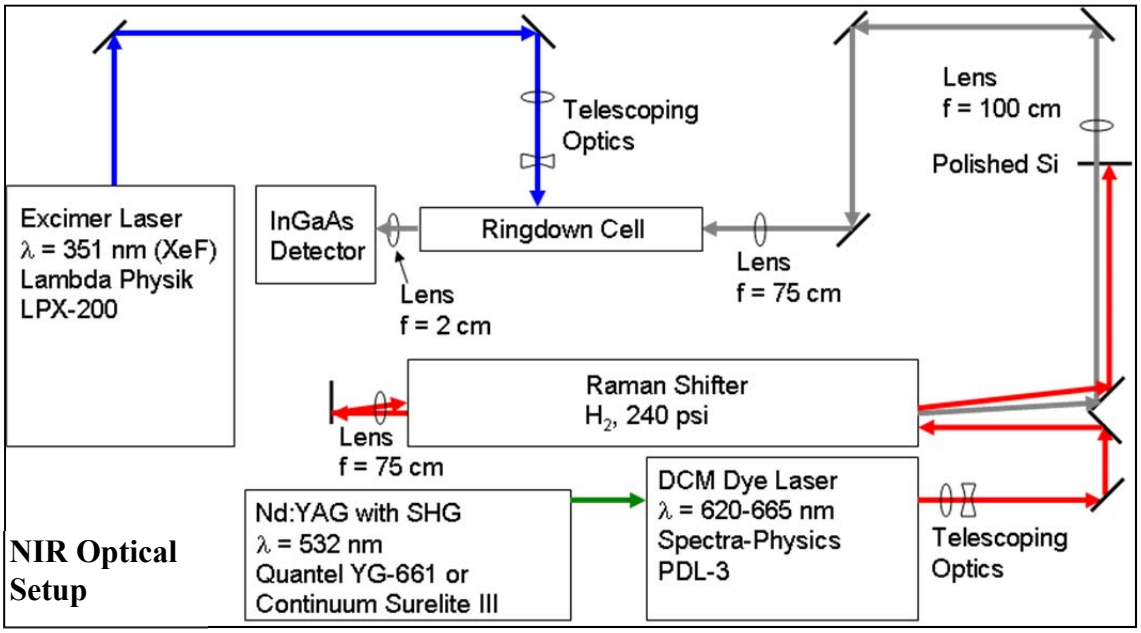

Figure 2.7. Optical setup for near-infrared light (1.2–1.4 μm, using the Raman shifter).

Gas kinetics cell

The first gas kinetics cell (used for the OH stretch measurements of $HOCH_2OO•$ described in Part 3) is illustrated in Figure 2.4. The gas kinetics cell was a 7 cm long stainless steel tube with a square cross section of 1 cm^2. The cell was coated with a fluoropolymer (FluoroPel PFC 801A/coFS) in order to prevent chemicals from sticking to or reacting with the cell walls. The sides of the cell had 6 cm long quartz windows to allow light to pass through for photolysis. The cell was coupled to the ringdown mirrors through Teflon blocks. The Teflon blocks also had gas ports to allow for introduction of gases to the cell. A pressure gauge (MKS Baratron) was attached to one of the Teflon blocks in order to monitor the pressure inside the cell.

The second gas kinetics cell (used for all other experiments described in this thesis) is illustrated in Figure 2.5. The gas kinetics cell was a 37 cm long quartz tube with a circular cross section of 1 cm^2. The cell contained three ¼" ports. Two of the ports were used for introduction of the sample gases and the vacuum system, creating a 5 cm sample length within the cell. A pressure gauge (MKS Baratron) was attached to the third port in order to monitor the pressure inside the cell. A quartz jacket around the central tube allows for heated or chilled solvent to flow around the sample. A flat quartz window on the front side of the solvent jacket allows light to pass through for photolysis, while ensuring a minimum of light is reflected off of the cell.

For all experiments, gas flows were measured by a set of mass flow transducers. Inert gases were sent through an Omega flowmeter, model number FMA1720 (brass, 0 to 10000 sccm), FMA1716 (brass, 0 to 2000 sccm), or FMA1712 (brass, 0 to 500 sccm). Corrosive gases were sent through an Edwards flowmeter, model number 831MF

(stainless steel, 0 to 1000 sccm) or model number 831MFT (stainless steel, 0 to 100 sccm). The voltage from each flowmeter was sent to both a digital display box and an SCSI card in the PC.

Optical Cavity

Ringdown mirrors (Los Gatos Research, Newport, ATFilms, Layertec) were placed in commercially available mounts (Los Gatos Research) and connected to the ends of the kinetics cell. The mirrors were placed 55 cm apart in the initial stainless steel cell (Figure 2.4), and 52 cm apart in the final quartz cell (Figure 2.5). Inert gas was flowed over the mirrors and through 24 cm long glass tubes to protect the mirrors from chemical damage. These tubes were coupled to the mirror mounts by UltraTorr adaptors.

Different mirrors were used in each spectral region. The mid-infrared mirrors (used for the OH stretch spectra described in Chapter 4) had a peak reflectivity of 99.975% at 2.8 μm. The near-infrared mirrors (used for the electronic spectra described in Chapter 3) had a peak reflectivity of 99.985% at 1.32 μm. Further details on mirror performance can be found in the "*Performance of Apparatus*" section.

Optical Parametric Amplifier Setup

Tunable mid-infrared (MIR) light over the range 2.7–3.7 μm was generated using an optical parametric amplifier (OPA) system similar to the one described by Reid and Tang.[47] The laser system is illustrated in Figure 2.6. The pump beam was 532 nm light obtained from second harmonic generation of a Nd:YAG (Quantel YG-661 or Continuum Surelite III) beam. While the YG-661 had a built in second harmonic generator, the

Surelite III did not. An external harmonic generator and crystal oven (Inrad 5-301) was installed to obtain 532 nm light. The lasers were run at a repetition rate of 10 Hz with a typical energy output of 160 mJ/pulse. 30%–50% of the 532 nm light was sent into a dye laser (Spectra Physics PDL3). DCM dye (4-dicyanomethylene-2-methyl-6-p-dimethylaminostyryl-4H-pyran) was used to generate tunable red light in the range 620-665 nm. The green and red laser beams were overlapped spatially and temporally, and sent through two potassium titanyl phosphate (KTP) crystals to generate infrared light in the range 2700–3700 cm^{-1}. The infrared light was tunable by adjusting the dye laser light frequency. The KTP crystals were connected to a stepper motor to allow for adjustment of the crystal orientation in order to maximize the infrared power at each frequency. The dye laser output and KTP crystal stepper motors were controlled using a LabView program. For typical energies of 160 mJ/pulse of 532 nm light, 9 mJ/pulse of red light was produced. Optical parametric amplification of these beams gave a typical infrared energy of 1 mJ/pulse. The linewidth of the light exiting the OPA was 1 cm^{-1}, limited by the linewidth of the 532 nm light (also 1 cm^{-1}).

Red and green light were separated from the infrared beam using sapphire optics with an antireflective coating. Remaining red light was removed by a polished silicon optic placed at Brewster's angle. The infrared beam was found to be slightly diverging. To correct for this, the beam was sent through a long focal length (75 cm) lens immediately prior to entering the optical cavity.

Raman Shifter Setup

Tunable near-infrared (NIR) light over the range 1.2–1.4 μm was generated using a hydrogen gas Raman shifter. The laser system is illustrated in Figure 2.7. The dye laser pump beam was 532 nm light obtained from second harmonic generation of a Nd:YAG (Quantel YG-661 or Continuum Surelite III) beam. While the YG-661 had a built in second harmonic generator, the Surelite III did not. An external harmonic generator and crystal oven (Inrad 5-301) was installed to obtain 532 nm light. The lasers were run at a repetition rate of 10 Hz. Typical 532 nm energy output of the Nd:YAG laser was 285 mJ/pulse for the YG-661, and 370 mJ/pulse for the Surelite III. All of the 532 nm light was sent into a dye laser (Spectra Physics PDL3). DCM dye was used to generate tunable red light in the range 620-665 nm. The red light was then telescoped to 0.5 mm beam diameter and sent through a two-pass Raman shifter (1.25 m per pass, 240 psi of H_2 gas). Lenses were placed in the optical path to ensure that the beam focused in the middle of the Raman shifter during both passes. The light was then passed through a polished silicon optic at Brewster's angle to isolate the near infrared (NIR) light produced from the 2nd Stokes shift (1.2–1.4 μm). For typical energies of 285 mJ/pulse of 532 nm light (YG-661), 20 mJ/pulse of red light was produced, leading to typical NIR light energies of 50 μJ/pulse. For typical energies of 370 mJ/pulse of 532 nm light (Surelite III), 30 mJ/pulse of red light was produced, leading to typical NIR light energies of 90 μJ/pulse. The linewidth of the NIR light was 0.1 cm^{-1}, limited by the linewidth of the dye laser (also 0.1 cm^{-1}).

Excimer Laser and Timing Control

Photolysis inside the gas cell was initiated by an excimer laser (Lambda-Physik LPX210i). For the experiments in this thesis, the gas mixture used was XeF, producing 351 nm light. The laser repetition rate was 10 Hz, with typical energies of 150–200 mJ/pulse. The laser beam size was 3 cm × 1 cm directly out of the excimer. The beam was focused vertically and expanded horizontally to a size of 5 cm × 0.3 cm before it entered the kinetics cell. Typical photon flux was 1.0×10^{17} photons cm^{-2}.

In order to determine the growth of spectral features with time, precise control over the relative fire times between the excimer and Nd:YAG lasers fire was required. To achieve this, the relative timing of the two lasers was controlled by two digital delay generators (Stanford Research Systems DG535). While the timing resolution of the delay generators is on the order of picoseconds, the overall timing precision of the experiment is determined by either the ringdown lifetime or relative timing jitter between the excimer and YAG laser pulses (whichever is larger). In the absence of jitter between the excimer and YAG pulses, the overall time resolution is 5 μs, equal to the ringdown lifetime. The resolution is worse (>10 μs) if significant timing jitter is present, as was the case when the YG-661 was installed incorrectly. See Appendix B for a detailed description of how the jitter between the excimer and YAG was eliminated.

Data Acquisition and Processing

Ringdown signals were detected by focusing the light exiting the optical cavity onto a photodiode detector with a short focal length lens. For the mid-IR experiments, an indium-antimony photodiode cooled to 77 K (InSb, Judson J10D-M204-R01M-60) was

used in conjunction with a 5 cm focal length CaF_2 lens. The signal coming out of the detector was sent through a voltage amplifier (Analog Modules 351A-3). For the near-IR experiments, a room temperature indium-gallium-arsenide detector (InGaAs, ThorLabs PDA-400) was used in conjunction with a 2 cm focal length CaF_2 lens. The PDA-400 has a built-in transimpedance amplifier, and no further amplification of the ringdown signal was necessary. For both sets of experiments, the amplified signal was sent through a ferrite choke and high pass filter before being sent to a PC oscilloscope board (GageScope CS1450). The sample rate of the card and data collection time were both dependent on the reflectivity of the cavity ringdown mirrors. Ringdown data were collected for 80 μs after the Nd:YAG laser fired at a sampling rate of 25 MS/s. Ringdowns from 16 or 64 shots (actual number dependent on the experiment) were averaged to obtain a ringdown trace. These traces were log-linear fit to obtain a preliminary ringdown lifetime. In order to reduce the effects of noise near the peak of the signal, data from the first 12.5% of the preliminary lifetime were cut. The remaining part of the trace was then refit using a Levenberg-Marquardt algorithm. All fitting was done in a LabVIEW program.[30]

Performance of CRDS Apparatus

Laser Performance

The tunable infrared light used to obtain cavity ringdown spectra is generated through multiple nonlinear processes. Therefore, it is critical that the lasers used to generate this infrared light are performing optimally. Three properties of the laser light must be classified: average pulse energy, pulse-to-pulse energy fluctuations, and timing

jitter (i.e., how much does the opening of the q-switch move in time, relative to the firing of the flashlamps). A low average pulse energy will reduce the signal-to-noise ratio for the ringdowns, while very large energy fluctuations or timing jitter will make it impossible to collect high-quality ringdown traces due to individual ringdowns exceeding the scale of the oscilloscope board.

Table 2.1 contains typical laser pulse energies and pulse-to-pulse energy fluctuations for each wavelength of light under operating conditions (1064 and 532 nm light from the Nd:YAG laser, 640 nm light from the dye laser, and the infrared light generated from the OPA and Raman shifter). A full report of performance at reduced energies (by reducing flashlamp voltage or by changing the q-switch delay time) as well as details on the methods used to classify laser performance can be found in Appendix A.

Table 2.1. Typical laser performance (energy per pulse, pulse to pulse 1σ energy fluctuation, and YAG timing jitter)

Pump Laser and Setup	1064 nm, YAG oscillator	1064 nm, YAG amplifier	532 nm, YAG SHG	640 nm, Dye	1.37 μm, Raman	2.8 μm, OPA	YAG Timing Jitter
Quantel YG-661*, OPA Setup	75 mJ	350 mJ	120 mJ	1 mJ	N/A	1 mJ	± 5000 ns
Continuum Surelite III, OPA Setup	394 mJ (±0.7%)	N/A	160 mJ (±2.2%)	9 mJ	N/A	1 mJ	± 8 ns
Quantel YG-661, Raman Setup	169 mJ (±0.5%)	625 mJ	285 mJ (±1.1%)	20 mJ (±5.0%)	51 μJ (±16%)	N/A	± 8 ns
Continuum Surelite III, Raman Setup	757 mJ (±0.25%)	N/A	376 mJ (±1.5%)	30 mJ	92 μJ (±20%)	N/A	± 8 ns

* YG-661 installed incorrectly while used with the OPA

It should be noted that the YG-661 was not functioning properly when experiments using the OPA setup were being performed. Energy fluctuations were quite large, due to fluctuations in the timing of the laser's q-switch and damage to the capacitor

bank. Repairs were made to the laser prior to using the YG-661 with the Raman shifter. Information about these repairs can be found in Appendix B of this thesis.

Detector Performance

It is important that the signal-to-noise ratio of the recorded ringdowns be as large as possible. The sensitivity of the instrument can be greatly improved simply by collecting and fitting the data over a large number of ringdown lifetimes. By choosing a detector appropriate for our laser power and ringdown mirrors, we can maximize our signal-to-noise ratio.

We can estimate the expected peak ringdown voltage as a function of mirror reflectivity. Comparing this value to the noise specification of the detector gives us a reasonable estimate of the signal-to-noise ratio. We first approximate the power reaching the detector as

$$P = \frac{E_{cavity}}{\tau_0} = \frac{(1-R)E_{IR}}{\left(\frac{L_{opt}}{c(1-R)}\right)}(X) = \frac{(1-R)^2 cE_{IR}}{L_{opt}}(X), \tag{2.8}$$

where P is the power reaching the detector, E_{cavity} is the IR energy stored in the ringdown cavity, τ_0 is the vacuum ringdown time, L_{opt} is the cavity length, c is the speed of light, R is the cavity ringdown mirror reflectivity, E_{IR} is the energy per pulse of the incident infrared light, and X is the fraction of light entering the cavity that actually couples to cavity modes. Given this approximation, the detector responsivity, and the detector amplification, the expected ringdown amplitude is

$$V_0 = \Re \times A \times P = \Re \times A \times \frac{(1-R)^2 cE_{IR}}{L}(X), \tag{2.9}$$

where V_0 is the ringdown amplitude, $\Re$ is the photovoltaic responsivity (in A/W), and A is the transimpedance amplification (in V/A).

The noise level for a detector can be calculated by Equation 2.10:

$$V_{noise} = \Re \times A \times NEP \times \sqrt{BW}\,, \tag{2.10}$$

where V_{noise} is the noise level in volts, NEP is the Noise Equivalent Power (watts $\text{Hz}^{-1/2}$), and BW is the detector bandwidth (Hz). NEP is proportional to the square root of the detector area, so smaller detectors will have less noise. For some detector/amplifier combinations (such as the PDA400), V_{noise} is directly reported in the spec sheet.

The detector properties and signal-to-noise ratio for the MIR and NIR setups are summarized in Table 2.2. Additionally, the number of ringdown lifetimes that can be measured before the ringdown signal falls below the noise is calculated via Equation 2.11:

$$\#\,\text{of lifetimes} = \ln\left(SNR\right) \tag{2.11}$$

where SNR is the signal-to-noise ratio. Each of the experimental setups (MIR, NIR) is expected to be capable of measuring at least 3.5 ringdown lifetimes before the signal falls below the detector's noise level.

Table 2.2. Expected ringdown peak voltages for MIR and NIR experiments

	Mid-IR (YG-661)	**Mid-IR (Surelite III)**	**Near-IR (YG-661)**	**Near-IR (Surelite III)**
Detector	Judson J10D-M204 (InSb, 77 K)	Judson J10D-M204 (InSb, 77 K)	ThorLabs PDA400 (InGaAs)	ThorLabs PDA400 (InGaAs)
Mirrors	Los Gatos, 2.8μ	Los Gatos, 2.8μ	Los Gatos, 1.35μ	Los Gatos, 1.35μ
Freq. (cm^{-1})	3620 cm^{-1}	3620 cm^{-1}	7540 cm^{-1}	7540 cm^{-1}
E_{IR} (μJ/pulse)	500	1000	15	90
L (cm)	55	55	60	60
R	0.9997	0.9998	0.9998	0.9998
$\Re$ (A/W)	3.0	3.0	7.5×10^3	7.5×10^3
A (V/A)	50	50	0.95	0.95
V_0/X (calc) (V)	3.68	3.27	4.80	28.8
V_0 (actual) (V)	0.145	0.075	0.277	1.2
X	0.04	0.02	0.06	0.04
NEP (W $Hz^{-½}$)	8×10^{-13}	8×10^{-13}		
BW (Hz)	3.5×10^6	3.5×10^6		
V_{noise} (V)	2.2×10^{-3}	2.2×10^{-3}	3.3×10^{-4} [a]	3.3×10^{-4} [a]
SNR	66	34	839	3636
# of lifetimes	4.2	3.5	6.7	8.2

a) Noise level reported directly on detector specification sheet

Mirror Reflectivity vs Wavelength

The cavity ringdown spectrometer's performance is intimately related to the reflectivity of the mirrors used. As seen in the previous section, a long ringdown lifetime allows for more data to be collected before the ringdown falls below the detector's signal-to-noise. In the center of the mirror's range, the reflectivity is the largest, and the ringdown lifetime will be longest. Further away from the central wavelength, the mirror reflectivity decreases, causing the ringdown lifetime to decrease. To properly classify the spectrometer performance, it is important to know the mirror reflectivity as a function of wavelength.

Equation 2.4 can be rearranged to solve for the mirror reflectivity:

$$R = 1 - \frac{L_{opt}}{c\tau_0}. \tag{2.12}$$

In order to determine the mirror reflectivity, vacuum ringdown data are recorded across the range of the mirrors. The ringdown lifetimes are then converted to mirror reflectivities via Equation 2.12.

The experiments described in this thesis used three sets of mirrors. The specifications for each set of mirrors are summarized in Table 2.3. The reflectivity curves for each set of mirrors can be found in Figure 2.8. The apparent dips in reflectivity observed in all of the reflectivity curves are due to water absorptions. Note that over time, mirror surfaces and coatings can become damaged, leading to a decrease in reflectivity. In particular, the Newport 1.35 μm mirrors suffered a large decrease in reflectivity over time, from 99.975% to 99.945%, as illustrated in Figures 2.8c and 2.8d. To avoid this phenomenon in the future, care must be taken to keep the mirrors as clean as possible to avoid the need for repeated washings.

Conversely, the Los Gatos 2.8 μm mirrors' reflectivity increased with repeated washings, from 99.97% in 2006 to 99.98% in 2011. This is a direct result of cleaning the mirrors carefully and purging the mirrors properly to avoid any contamination during experiments. Thus, one should not be afraid to clean the mirrors when necessary.

Table 2.3. Summary of cavity ringdown mirror specifications

Manufacturer	**Los Gatos 2.8 μm**	**Los Gatos 1.32 μm**	**Newport 1.35 μm**
Peak Reflectivity	99.975%	99.985%	99.975%
Mirror Center	3300 cm^{-1}	7590 cm^{-1}	7280 cm^{-1}
Mirror Range	2900–3800 cm^{-1}	7100–8000 cm^{-1}	6900–7800 cm^{-1}

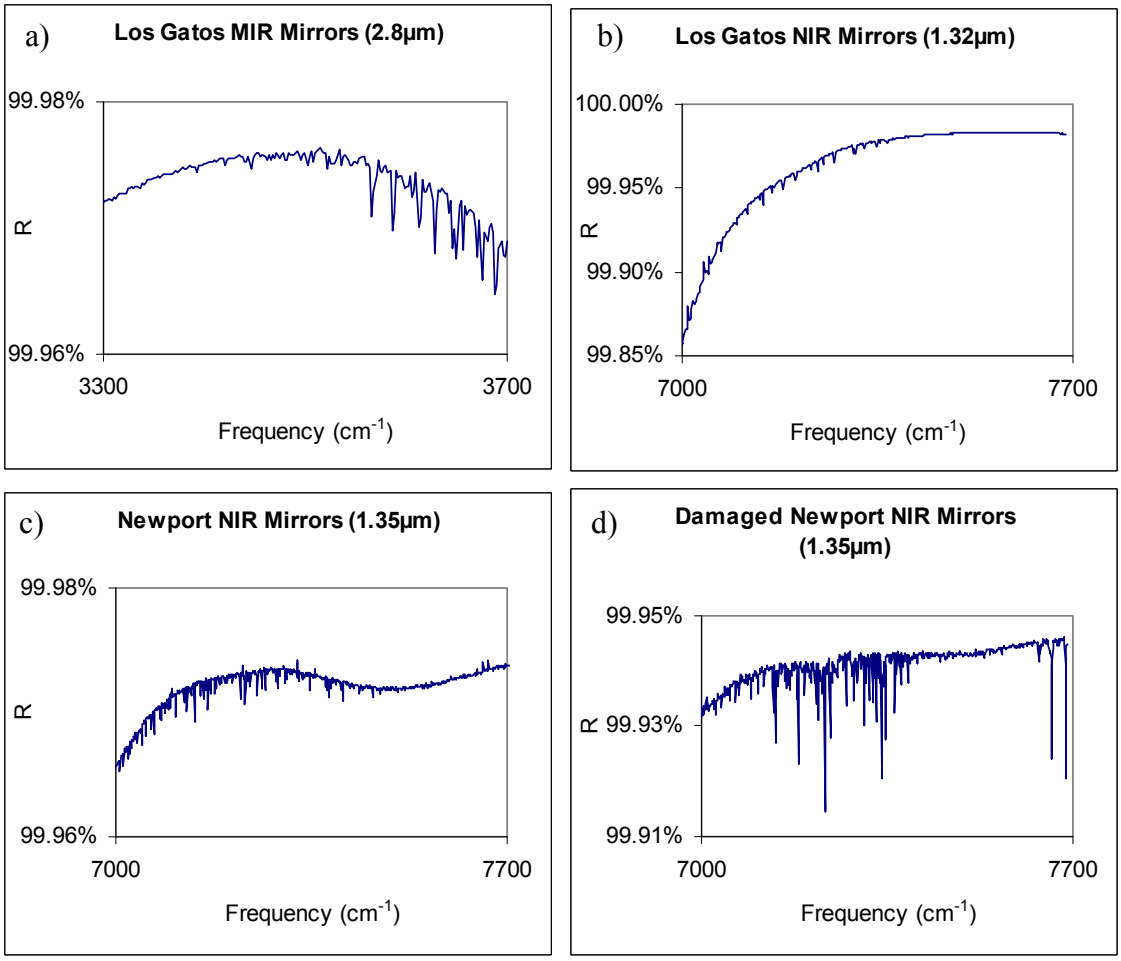

Figure 2.8. Reflectivity curves for the cavity ringdown mirrors used in this thesis: Los Gatos mirrors centered at 2.8 μm (a), Los Gatos mirrors centered at 1.32 μm (b), Newport mirrors centered at 1.35 μm (c), and damaged Newport mirrors centered at 1.35 μm (d). The apparent dips in reflectivity are due to absorptions by water.

It is not practical to simply use the most reflective mirrors available in the apparatus. As the mirror reflectivity increases, the ringdown lifetime also increases, which should result in the ability to fit larger amounts of data, increasing the effectiveness of the spectrometer. However, the relationship between mirror reflectivity and ringdown amplitude in Equation 2.9 also needs to be considered:

$$V_0 = \Re \times A \times \frac{(1-R)^2 \, cE_{IR}}{L}(X). \qquad (2.9)$$

If the mirror reflectivity (R) is too high, then not enough light will be able to enter the cavity, and the peak ringdown voltage (V_0) will become too small to detect. It is therefore important to choose mirrors with a high enough reflectivity to create large ringdown times, while simultaneously transmitting enough light to be detected.

It is also important to consider the detector's responsivity ($\Re$) and amplification (A) when choosing mirrors. If $\Re$ and A are large, then smaller signals can be detected, and more highly reflective mirrors can be used. However, one should not simply choose a detector with the highest $\Re$ and A available. As the detector's amplification increases, the detector bandwidth will decrease. If the bandwidth is too small, then the recorded ringdowns will be distorted. Typically, the bandwidth of the detector must be greater than $5/\tau$ in order to avoid this effect. For our experiments, the minimum acceptable detector bandwidth is approximately 3 MHz.

Sensitivity of the CRDS Apparatus

In theory, the exact ringdown lifetime can be calculated given knowledge of the mirror reflectivity, absorber concentrations, and absorbance cross sections. In practice, small changes in cavity length, mirror alignment, sample composition, and imperfect ringdown fitting cause a statistical scatter in measured ringdown lifetimes. The size of this statistical scatter can be used to determine the minimum detectable absorbance, via Equation 2.6:

$$A = \frac{L_{opt}}{c}\left(\frac{1}{\tau} - \frac{1}{\tau_0}\right). \qquad (2.6)$$

Suppose a large number of ringdowns are collected and fit at a particular wavelength. The ringdown times have an average value $1/\tau_0$ and standard deviation $\sigma_{1/\tau 0}$. The relative standard deviation (labeled as $\Delta\tau/\tau$) is given by Equation 2.13:

$$\frac{\sigma_{1/\tau_0}}{1/\tau_0} = \frac{\Delta\tau}{\tau}. \tag{2.13}$$

For the experiments in this thesis, the minimum detectable absorbance ($A_{\min}$) corresponds to 2 standard deviations in absorbance (σ_A), or

$$A_{\min} = 2\sigma_A = \frac{2L_{opt}}{c}\left(\frac{\Delta\tau}{\tau}\right)\left(\frac{1}{\tau_0}\right). \tag{2.14}$$

It can be observed that $\Delta\tau/\tau$ generally remains constant regardless of the ringdown lifetime τ_0. Thus, $\Delta\tau/\tau$ can be considered a wavelength-independent measure of spectrometer performance. Additionally, $\Delta\tau/\tau$ should behave statistically with respect to the number of averaged ringdowns per trace (N):

$$\frac{\Delta\tau}{\tau} \propto \frac{1}{\sqrt{N}}. \tag{2.15}$$

Equation 2.14 also reveals one other key idea: $A_{\min}$ is proportional to $1/\tau_0$. This means that the sensitivity of our apparatus will decrease if the reference ringdown time is too small. It is therefore important to keep the background $1/\tau_0$ small by choosing precursor chemicals with small absorbances in the spectral region being measured.

The MIR setup typically had a $\Delta\tau/\tau$ of 0.4% (16 shots averaged) with the Los Gatos 2.8μm mirrors, leading to a minimum detectable absorbance of 2.6 ppm $Hz^{-½}$. The NIR setup typically had a $\Delta\tau/\tau$ of 0.2% (16 shots averaged) with the Los Gatos 1.32μm mirrors, leading to a minimum detectable absorbance of 0.8 ppm $Hz^{-½}$. It was observed

that increasing the fitting window from 40 μs to 80 μs was the most important factor in reducing $\Delta\tau/\tau$, likely because the baseline for the ringdown is better defined. However, further increases to the fitting window will not improve $\Delta\tau/\tau$. At longer times than 80 μs, the ringdown trace will fall below the detector noise level.

Calibration of Spectrometer Frequency

Spectroscopic measurements are of limited value without precise knowledge of the frequency of light being used. In general, a spectrometer must provide some means of determining the wavelength of light being used. There are two approaches to this calibration: external equipment to verify the frequency of light being used, or measurement of internal standard compounds within the spectrometer. Many spectrometers make use of atomic lamp absorptions as a means of externally measuring the dye laser frequency.[50, 51] This technique is sufficient for Raman shifter setups, since the dye laser light and the Raman shift of H_2 are the only factors determining the wavelength of the IR light. However, the atomic lamp technique is not acceptable when using an OPA, because the frequency of the light from the YAG also affects the final IR wavelength. If the YAG is not precisely at 532 nm, then the calculated and actual IR frequencies out of the OPA will be different.

Rather than attempt to simultaneously measure the frequencies YAG and dye laser light, we measure the spectra of known absorbers within our cavity ringdown spectrometer in order to determine the frequency of IR light. A numerical readout on the dye laser indicates the position of its diffraction grating. By measuring well-known spectroscopic bands, we observe that the relationship between the numerical readout and

the wavelength of light produced is constant (within 0.1 cm^{-1}, the linewidth of the dye laser). Two different, stable (i.e., nonradical) absorbers are required for each setup (OPA, Raman). By using two separate absorbers, we are able to calibrate the absolute position as well as the dye laser motor step size.

For the OPA setup (2.7–3.7 μm), we used the $2\nu_2$ band of formaldehyde (3471.7 cm^{-1})[52, 53] and the ν_1 band of water (3657 cm^{-1}) [40] to calibrate the spectrometer. The calibration was confirmed by measuring band positions of H_2O_2 (ν_1=3609 cm^{-1}, ν_5=3618 cm^{-1}) and *n*-butanol (ν_1=3675 cm^{-1}).[40] For the Raman shifter setup (1.2–1.4 μm), we used the $2\nu_1$ band of methanol (7199 cm^{-1})[40] and the $\nu_1+4\nu_4$ band of HCHO (7374 cm^{-1}).[52, 53] The calibration was confirmed by the A-X electronic transition of HO_2 (7029.4 cm^{-1}).[54, 55]

Conclusions

We have installed and characterized a pulsed laser photolysis-cavity ringdown spectrometer in order to study the spectroscopy and kinetics of atmospherically relevant chemical species. Tunable infrared light is generated using an optical parametric amplifier (2.7–3.7 μm) or a Raman shifter (1.2–1.4 μm), pumped by pulsed Nd:YAG and dye lasers. Photolysis of the chemical reactants is achieved by sending light from an excimer laser through the cavity ringdown cell. The instrument is capable of measuring absorptions as low as 2.6 ppm $Hz^{-½}$ (mid-IR) or 0.8 ppm $Hz^{-½}$ (near-IR), with a time resolution of 5 μs. The spectrometer has been calibrated along its frequency axis by measuring known spectroscopic bands. With the spectrometer verified to be in good

operating condition, we now turn our attention to the specific chemical systems discussed in Chapter 1.

Acknowledgements

We thank Eva R. Garland and Todd L. Fuelberth for construction of the OPA stage, Andrew K. Mollner for installation of the excimer laser and gas lines, David J. Robichaud for LabVIEW programming, Dave Natzic for machining the ends of the Raman shifter, Rick Gerhart and Mike Roy for construction of the gas kinetics cells, and Ralph H. Page for improvements to the optical setup. The apparatus described in this chapter were funded under NASA Upper Atmosphere Research Program Grants NAG5-11657, NNG06GD88G, and NNX09AE21G2, California Air Resources Board Contract 03-333 and 07-730, and a Department of Defense National Defense Science and Engineering Graduate Fellowship (NDSEG).